# Crack initiation and growth in PV module interconnection

Alireza Eslami Majd*, Nduka Nnamdi Ekere

*School of Engineering, Faculty of Science and Engineering, University of Wolverhampton, UK*

## ARTICLE INFO

## ABSTRACT

As the cost of PV (photovoltaic) solar panels drops, it is widely expected that solar energy will become the cheapest source of electricity in many parts of the world over the next two decades. To ensure that PV solar modules have a long service life and can meet the PV manufacturer's warranty, the PV modules need to have high reliability. Solar PV module manufacturers typically provide two warranties: a performance warranty which guarantees 90% of original power output after 10 years and 80% of original output of at 25 years; and an equipment warranty which guarantees their PV module will have a minimum of 10–12 years operation before failure. A critical part of the solar PV module assembly is the ribbon interconnection between the solar cells (i.e. the solder joint interconnections), and failure of the ribbon interconnection can adversely affect the performance and reliability of whole PV module. Ribbon interconnection failures have been linked to the thermal cracks which are initiated in the solder joint material during the high temperature ribbon interconnection manufacturing process; and then the crack propagation and growth associated with the thermal cycling of the ribbon interconnections under higher than ambient temperature PV module operating conditions. This paper reports on the study of high temperature crack initiation and propagation in different PV Module interconnection configurations by using XFEM in ABAQUS software. It concerns a necessary, urgent and fundamental revision of the manufacturing process that lies at the heart of PV module ribbon interconnection manufacture.

## 1. Introduction

With massive investments in renewable energy in recent years, renewable energy is establishing a strong foothold in the global energy system at a faster rate than any other fuel source in history - and for this reason renewable energy is expected to become the world's main source of power within two decades. Indeed, the International Energy Agency (IEA) 2014 Technology Roadmaps for Solar Photovoltaic Energy and for Solar Thermal Electricity concluded that solar energy could surpass fossil fuels, wind and hydro by 2050 to be the world's largest energy source. This is because generating electricity from solar energy, an abundant and renewable source, using photovoltaic (PV) systems has become very widespread. This increase in the use of photovoltaic (PV) solar systems for generating electricity has been driven by subsidy programs and economic incentives for investments by several governments. Due to the increased economic incentives, the worldwide growth of solar PV has been close to exponential between 1992 and 2018; thereby helping solar PV technology to evolve from a niche market of small scale applications to a mainstream electricity source. This growth in PV solar is set to continue, according to the IEA's latest 5-year forecast, renewable power capacity is set to expand by 50% between 2019 and 2024, led by solar PV (IEA, 2019).

The solar PV cells (panels) technology has been used in several applications over the years (for example, they have been utilised successfully as an energy source on rooftops, spacecraft, handheld calculators and other wearable electronic devices). The motivation for this study is to investigate novel PV Module interconnection configurations which can improve the PV module power output by increasing the incidence of light onto the PV solar module also improve ribbon interconnection reliability.

### 1.1. Reliability of PV modules

Unlike other electrical equipment, PV modules are unique in that they carry very long-term performance warranties of 20–25 years (indeed, very few types of electrical equipment have such long warranties) and for this reason, improving the reliability of PV modules remains a major R&D challenge. As reliability is neither defined nor covered by the existing quality certification standards such as the IEC 61215 (IEC International Electro Technical Commission), it follows that using the design qualification to these standards does not imply the PV module's reliability. This lack of reliability standards is partially due to the fact

that PV solar module technology is still in its infancy (with most PV installations yet to reach their 20–25 year lifetime as per warranty), and thus there is very little or no statistical data available on PV module field failure (Ferrara & Philipp, 2012), (Ishii & Atsushi, 2017). This study concerns a necessary, urgent and fundamental revision of the soldering process that lies at the heart of PV module ribbon interconnection manufacture. Through a new methodology, it addresses the modelling of the impact of different PV Module interconnection configurations on the crack initiation temperatures and crack growth rates for improved PV Module interconnection reliability.

The ribbon interconnection of the PV solar module is critically important component. The ribbon interconnection is soldered directly onto silicon crystals to interconnect solar cells in the PV module and it plays an important role in determining cell efficiency, as it serves to carry the current generated in the solar cells to the PV busbar. The ribbon solder interconnection has been reported as the part of the PV module system that is most susceptible to failure, and hence the dominant factor in PV module degradation and is responsible for over 40% of recorded field PV module failures (Herrmann, 2010). Also in their validation of the PV life model using 3 million module-years of live field data, Hasselbrink, et al. comprehensively reviewed the customer fleet returns sheets focussing on the reasons for returns due to failure over an average deployment period of 5 years; and they found that circa 66% of the returns were due to solder interconnection failures, whilst encapsulate and back-sheet failures accounted for circa 22% of returns (Hasselbrink, et al., 2013).

A number of studies on the analysis of crack in the PV module Silicon material has been reported, notably the investigation of the cracks in Silicon layers exposed to thermal cycling and to mechanical loading (M. Sander et al., 2011). Their study shows that cracks were observed mainly at the beginning and the end of the busbars and that the cracks grow along the length of the busbars. However, there are no reports of previous studies on the crack initiation and growth in the interconnection material of PV modules and on PV interconnections design to improve the reliability. For this reason, the focus of recent PV module reliability studies has been on the ribbon interconnection design and failure. These include some experimental studies focussed on the investigation of the failure mechanism of the ribbon interconnection and this shows that the solder coating on the ribbon interconnection is the most common source of failure. The ribbon interconnection failure is mostly linked to crack initiation and propagation in the solder joint material which exhibits brittle mechanical behaviour. The nucleated crack in the solder joint can lead to hot spots due to the high contact resistance at the ribbon and the cell interface and then potentially results in DC arc (Itoh, et al., 2014). In addition, these hot spots can also lead to the degradation of the encapsulation and partial shading effects; consequently this problem impacts on the performance parameters and reduces power outputs and the efficiency of the PV module (Bidram, et al., 2012) and (Pareek, et al., 2017).

Very few of the studies reported on the analytical and/or numerical investigation of the failure of the PV module interconnection (solder joint) have considered the modelling of nonlinearities as most studies have only assumed linearity and early elastic states. (Wang, et al., 2016). Equally, in their consideration of the influence of the coefficient of thermal expansion (CTE) of the PV module materials on the stress level, most studies have assumed linear and temperature independent behaviour. Hence, the focus of this study is to incorporate nonlinearities and temperature dependence in the investigation of the impact of ribbon interconnection design on the failure and reliability of PV solar modules.

### 1.2. Problem context

In spite of the best efforts of manufacturers to minimise and control thermomechanical stress effects on the PV module, the high temperature process can lead to micro-cracks in the solder joint material of the

ribbon interconnection and the cells, which can lead to crack nucleation and propagation and subsequent interconnection failure. This can be explained by the fact that during the hot temperature manufacturing process, the coefficient of thermal expansion (CTE) mismatch (between interconnecting materials) results in high levels of stress and strain; and this accumulation of strain energy is responsible for the initiation of micro-cracks in the solder joint materials.

Experimental studies have shown that with high temperature cycling of PV modules (such as those experienced by PV modules during in high temperature climates), the micro-cracks initiated in the solder joint material can grow and propagate through the connecting layer and ultimately lead to PV module failure. This is particularly true with lead-free solder joint materials (which is now the preferred environment-friendly joining material), as these have higher probability of developing micro-cracks due to their lower fracture strength and higher thermo-mechanical stress levels when compared to tin-lead solder alloys (Pander, et al., 2014).

### 1.3. Solder fracture

A number of previous studies have reported on the fracture mechanics and the effect of solder joint geometry on the reliability of electronics assembly board interconnections subjected to thermo-cycling loads. These include the development of an empirical equation for predicting the thermal-fatigue life of solder bumps using the measured crack growth rate at the crack tip (H. Lau, et al., 2001); the prediction of the effect of solder joint geometry on the reliability of Ball Grid Array (BGA) solder joints on flexible and rigid PCBs subjected to thermo-cyclic loading (Lau, et al., 2014); the investigation of the impact of Inter Metallic Component (IMC) on the reliability of lead-free solder joints at elevated temperature operations (Amalu and Ekere, 2011) and modelling evaluation of Garofalo-Arrhenius creep relation for lead-free solder joints in surface mount electronic component assemblies (Amalu and Ekere, 2016). The results of these previous studies show that the thermal fracture mechanism of a solder joint interconnection can generally be sub-divided into two distinct modes. Firstly, the fractures that occur inside the solder joint due to solder grain size growth and the corresponding decrease in bonding strength during thermal cycling, which then leads to crack propagation at the interface of large grains. Secondly, the fractures that occur at the interface of solder with interconnection material (that is within the Inter Metallic Component (IMC) layer formation); for example $Cu_5Sn_6$ and $Ag_3Sn$ which is formed through the dissolution of the Ag/Cu materials in the solder (Itoh, et al., 2014). A recent study on the investigation of the effect of non-homogenous solder coating on the micro-crack initiation temperature in the round wire Multi-Busbars of the PV solar module showed that the crack nucleates at the edge of the IMC layer; and the interface between the solder joint and silver pad (Eslami Majd & Ekere, 2019). Another simulation study shows that higher strain rates and thicker IMCs results in IMC-interface brittle fracture or IMC-controlled fracture; whilst lower strain rates and smaller IMC thickness leads to solder-internal fracture or solder-controlled fracture (Fei, et al., 2012). Results from a study on the analysis of experimental samples have shown that the Ag to solder crack in IMC region is more prevalent than the Cu to solder region crack (Jeong, et al., 2012), whilst the studies by Li, et al showed that fractures and the straight crack propagation path tends to be located on the component side of the solder interconnections - beneath die edge (Li, et al., 2012); and that the tensile and the shear strength of IMC layers decrease with increase in the IMC layer thickness (Zhong, et al., 2010).

In this Study, we investigate the micro-crack initiation and growth in the lead free solder joint material of the conventional PV Module ribbon interconnection during the high temperature manufacturing process. The results of this study will be beneficial for researchers in predicting the propagation paths for existing micro-cracks during the thermal fatigue cycling under in-service PV module operating

conditions; and hence for the prediction of PV Module interconnection reliability. The XFEM in ABAQUS Software was used for this study as it enables the accurate solution of boundary value problems with discontinuities and singularities freely located within elements of the mesh (Fries, 2018). The XFEM facilitates stress intensity factor computations even on relatively coarse meshes, and further-more, no re-meshing is required for crack growth simulations.

## 2. Finite element modelling and simulation

The Extended Finite Element Method (XFEM) feature of the ABAQUS 2019 is employed for determining the critical temperature for micro-crack initiation and growth in PV module ribbon interconnections. The XFEM is based on the generalized finite element method (GFEM) and the partition of unity method (PUM), and this numerical technique extends conventional finite element method and allows local enrichment discontinuous functions to be combined with the numerical approximation. Unlike ordinary FE methods, with the XFEM method there is no need to define the crack location beforehand. In effect, the XFEM models a crack within an enriched element by adding degrees of freedom in elements with special displacement functions. This means that while XFEM is generating discontinuous fields along a crack and around its tip, there is no need for modelling the geometry of the crack and for re-meshing in the simulation (ABAQUS, 2017). The detailed formulations and further information for XFEM can be found in (Mohammadi, 2008) and (Moës, et al., 1999).

The methodology and steps applied to the XFEM in ABAQUS software are firstly validated by comparison with the experimental results to form the tension test of dogbone specimen. Comparison of the results showed good agreement for Force-Displacement curve; then, the defined setups have been used for the simulations in ABAQUS software.

### 2.1. Structure and geometry of models

Fig. 1 shows the schematic view of the assembly of the ribbon interconnections between solar cells in the PV module assembled by back to front connection method. The PV solar module is typically built up of different materials, including: silicon as the semiconductor material, EVA (ethyl vinyl acetate) which serves as encapsulate materials to protect solar cells, aluminium sheet to envelop the backside of the silicon, the pasted silver pads and fingers to receive the electrical current, Tedlar (Polyvinyl Fluoride) as a back sheet to cover the bottom, glass as front cover and the copper wire coated with solder materials to collect the electrical current from the individual cell.

In this study the thickness of aluminium, silicon cell, EVA, glass and Tedlar layers used for the FE models are assumed to be 25 μm, 200 μm, 460 μm, 3 mm and 190 μm, respectively. The thickness of other component parts such as silver pad, copper, solder used and the ribbon interconnection width have been varied to investigate the effect of ribbon interconnection geometry and design on the crack initiation and propagation parameters.

Also, in this study to take account of the high ratio of the ribbon interconnection length to the other dimensions of model, the 2D plane-strain elements (CPE3[1] and CPE4[2]) have been used to increase the computational solution speed. The symmetry boundary condition is applied to the mid-point of the ribbon interconnection section and bottom-end of the Tedlar material is closed. Fig. 2, presents the schematic view of ribbon interconnection FE model; showing the boundary conditions, the arrangement of component materials and the meshing style (**Note**: the fine meshing technique is used for the crack area in the solder joint material).

---

[1] A 3-node linear plane strain triangle
[2] A 4-node bilinear plane strain quadrilateral

### 2.2. Load condition

In this study, the thermal load is applied uniformly to the model as the temperature of all components of the PV module is assumed homogenous and the temperature is applied linearly by increments of 15 °C per minute.

### 2.3. Material properties

The mechanical properties of the materials used in the simulation are presented in Table 1. For metallic materials, plastic behaviour has been assumed and linear elastic behaviour is assumed for the IMC layer (due to its brittleness). Based on cohesive traction-separation law method, the maximum nominal stress (MAXS) in the shear and tensile directions are considered as the controlling parameters for the damage initiation in the IMC layers. This means that the damage (crack) is initiated when these components exceed the defined limits, and then the initiated crack will be evaluated as a function of the fracture energy. For a more realistic simulation, we investigate the effect of temperature dependence of important material properties, such as the coefficient of thermal expansion of silicon and metallic materials and the Young's Modulus and plastic behaviour of the solder joint material (see Table 2).

## 3. Results and discussion

This section presents the results and analysis of the simulation modelling for different PV module ribbon interconnection configurations and design parameters. The crack location, the crack initiation temperature and crack propagation rate are determined for each state. Our results show that the crack initiation temperature and crack propagation rate are dependent on the dimensions of ribbon interconnection. The effect of different PV module ribbon interconnection configurations and design parameters on the crack initiation temperature and crack propagation rate are presented in the sub-sections below.

### 3.1. Effect of changing solder and IMC thickness

The results from the FEM simulation showed that increasing the solder coating thickness leads to a decrease in the crack initiation temperature (circa linear relationship); and this reduction in crack initiation temperature is more pronounced for thicker IMCs (see Fig. 3). This can be explained by the higher stress levels in the solder joint material and the strain accumulation in the IMC layer which results in crack initiation at lower temperatures. This result is not in line with the expectation that a thicker solder coating will result in higher interconnection reliability (a stronger solder joint that will be more resilient to premature failures).

Fig. 4 presents a plot of the effect of solder coating and IMC thickness on the crack growth rate. The results show that the crack growth rate is almost constant for the solder coating thickness less than 50 μm, but further increases in solder coating thickness beyond the 50 μm limit leads to a big jump in the crack growth rate. Fig. 4 also show that the crack growth rate is much lower in the thicker IMC layers compared to thinner IMC layers.

As can be seen in Fig. 5, for all the simulation results presented in Fig. 3, the location for the crack nucleation is at the edge of IMC layer interface with the copper ribbon and the propagation is in the shear direction; as the shear strength of the IMC layer material is lower than its tensile strength.

Based on the results presented in Fig. 3 and Fig. 4, a solder coating thickness of between 20 μm and 30 μm is recommended as this will help to keep the crack growth rate low and also keep the crack initiation temperature high; helping to increase the PV ribbon interconnection reliability.
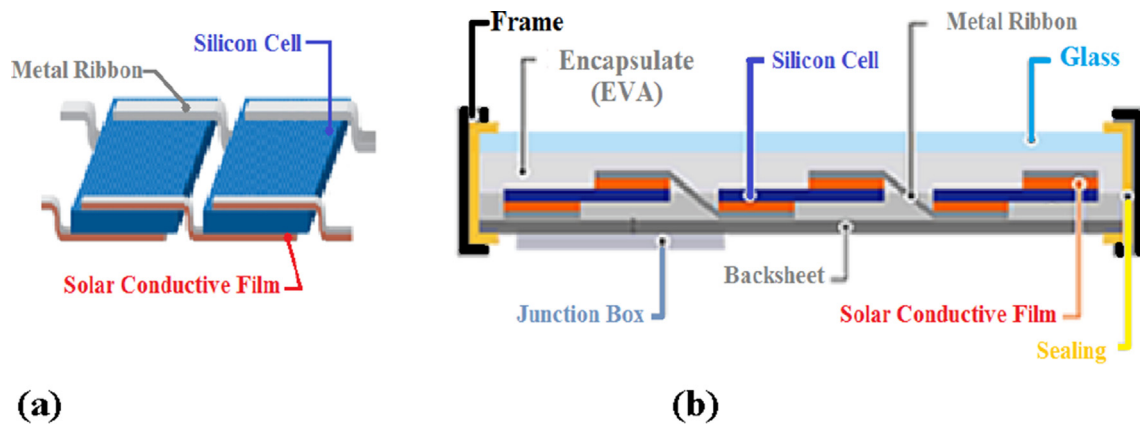
**Fig. 1.** Ribbon interconnections assembly between cells in the PV Module (a) Side view of cross section of PV modules included Materials (b).
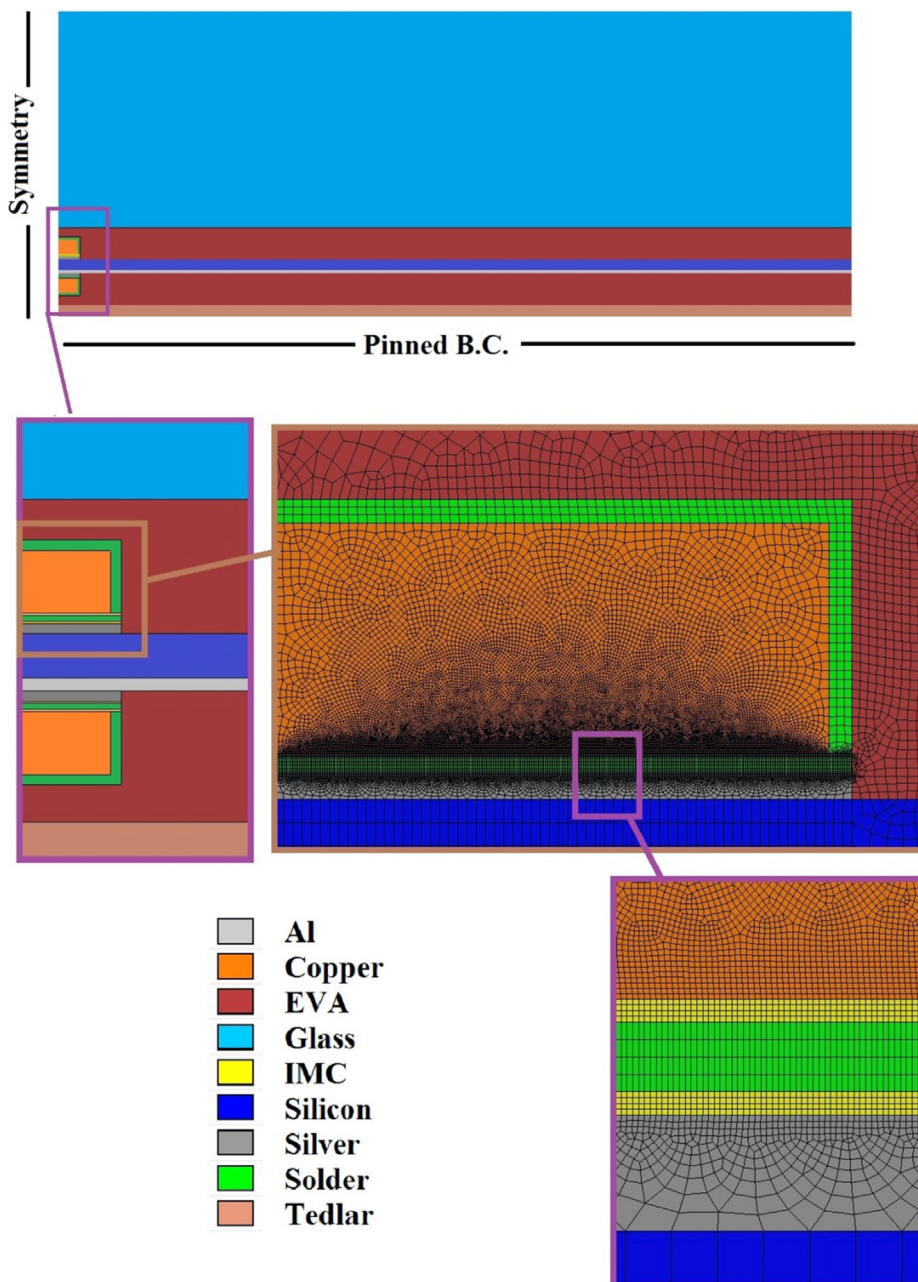


**Fig. 2.** Schematic view of 2D simulation of ribbon interconnection with showing boundary conditions, mesh styles and arrangement of materials.

**Table 1**
Mechanical Properties of Material used in the FEM simulation of ribbon interconnection.

| Parameter (unit) | Material | | | | | | | | |
|---|---|---|---|---|---|---|---|---|---|
| | IMC (Deng, et al., 2005) & (Zhong et al., 2010) | Solder Joint | Silver (AZoM, 2001) | Copper (Jing, et al., 2015) | EVA (Cambridge University Engineering Department, 2003) | Silicon (Owen-Bellini, et al., 2015) | Aluminium (AZoM, 2005) | Tedlar (DuPont™, 2014) | Glass (Tippabhotla, et al., 2017) |
| Elastic Modules (GPa) | 110 | See Table 2 | 69 | 121 | 11 | 130 | 68.3 | 2.138 | 73.0 |
| Poisson's Ratio (-) | 0.3 | 0.35 | 0.365 | 0.34 | 0.499 | 0.28 | 0.34 | 0.4 | 0.235 |
| Yield Stress (MPa) | – | – | 43 | 121 | 12 | 170 | 85 | 41 | – |
| Shear Strength (MPa) | $27.6–1.95*H_{IMC}$ | 30 | 120 | 248 | 16 | – | 60 | – | – |
| Tensile Strength (MPa) | 65 | 78 | 120 | 248 | 16 | – | 100 | – | – |
| Fracture Toughness (MPa.m^0.5) | 1.4 | 7 | 40 | 30 | – | 0.83 | 22 | – | – |
| Thermal Expansion Coefficient (ppm/k) | See Table 2 | See Table 2 | See Table 2 | See Table 2 | 270 | See Table 2 | See Table 2 | 78 | 8.0 |
| Plastic Stress-Strain Curve (MPa) | – | See Table 2 | 43@0.001 120@0.04 | 121@0.001 186@0.004 217@0.01 234@0.02 248@0.04 | – | – | 85@0.00 100@0.12 | 41@0.00 55@0.9 | – |

**Table 2**
Temperature dependent properties of interconnection materials.

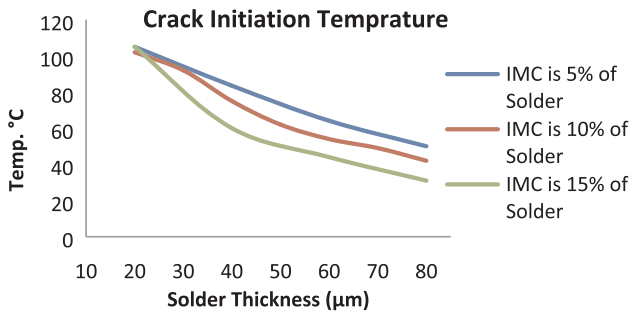| Temp. (°C) | CTE for Copper (ppm/k) (Taulaukian, et al., 1975) (Interpolated) | CTE for Silicon (ppm/k) (Sasi Kumar, et al., 2017) (Interpolated) | CTE for Silver (ppm/k) ((Taulaukian, et al., 1975) (Interpolated) | CTE for Aluminium (ppm/k) (Taulaukian, et al., 1975) (Interpolated) | CTE for IMC (ppm/k) (Jiang, et al., 1997) (Interpolated) | CTE for Solder (ppm/k) (21.3 + 0.017 T) (Li, el al., 2012) | Solder Young's Modulus (GPa) (49–0.07 T) (Li et al., 2012) | Plastic Stress for Solder (MPa) (at 0.0, 0.065 Plastic Strain) (Siviour, et al., 2005) (Interpolated) |
|---|---|---|---|---|---|---|---|---|
| 0 | 16.22 | 2.35 | 18.67 | 22.50 | 17.7 | 21.3 | 49 | 71, 145 |
| 30 | 16.60 | 2.63 | 18.98 | 23.29 | 18 | 21.81 | 46.9 | 52, 131 |
| 60 | 16.91 | 2.87 | 19.20 | 23.85 | 18.3 | 22.32 | 44.8 | 16, 110 |
| 90 | 17.22 | 3.04 | 19.42 | 24.41 | 18.6 | 22.83 | 42.7 | – |
| 120 | 17.53 | 3.20 | 19.65 | 24.97 | 19 | 23.34 | 40.6 | – |
| 150 | 17.76 | 3.36 | 19.91 | 25.40 | 19.8 | 23.85 | 38.5 | – |

**Fig. 3.** Effect of solder and IMC thickness on the crack initiation temperature (Silver thickness, copper thickness and ribbon breadth are considered as 50 μm, 200 μm and 1 mm, respectively).
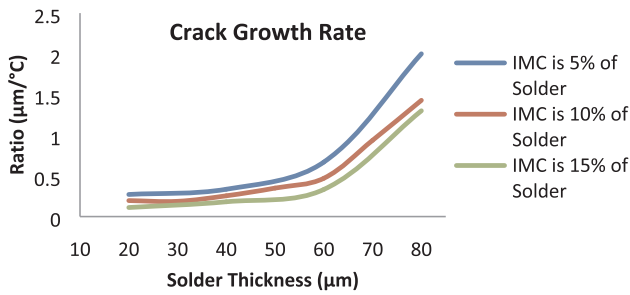


**Fig. 4.** Effect of solder and IMC thickness on the crack growth rate (Silver thickness, copper thickness and ribbon breadth are considered as 50 μm, 200 μm and 1 mm, respectively).
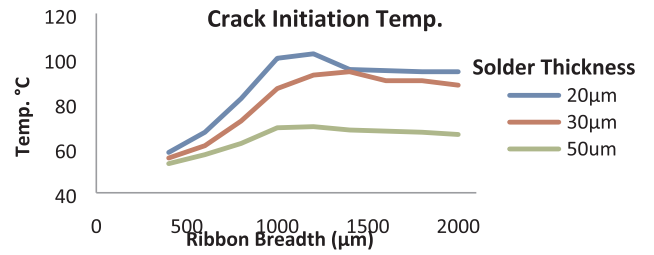


**Fig. 6.** Effect of ribbon breadth on the crack initiation temperature for different solder thicknesses (Silver thickness, copper thickness and IMC thickness are considered as 50 μm, 200 μm and 4 μm, respectively).
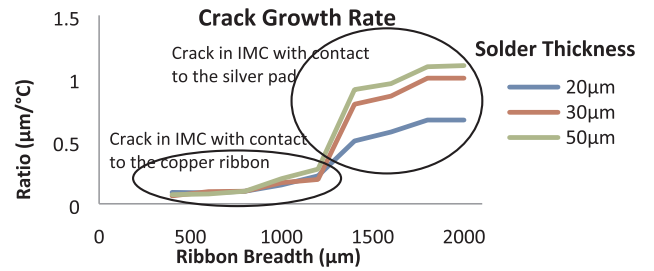


**Fig. 7.** Effect of ribbon breadth on the crack growth rate for different solder thicknesses (Silver thickness, copper thickness and IMC thickness are considered as 50 μm, 200 μm and 4 μm, respectively).

width limit. The reason for this sharp increase in crack growth rate is
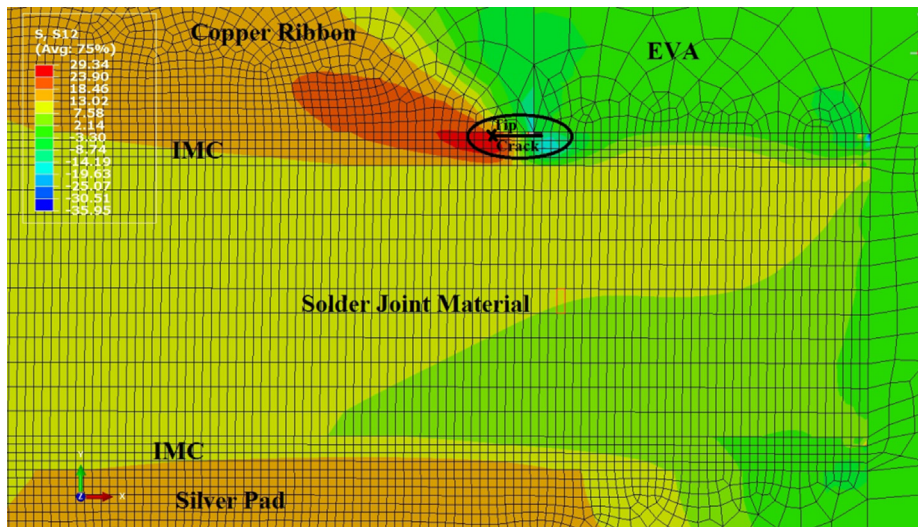


**Fig. 5.** Crack's location and propagation direction in the IMC layer interface with the copper ribbon (Shear stress distribution contour is displayed).

### 3.2. Effect of ribbon breadth change

Fig. 6 and Fig. 7 show the effect of changing the ribbon width on the crack initiation temperature and crack growth rate, respectively, for different solder thicknesses. Our results presented in Fig. 6 show that increasing the ribbon width leads to an increase in the crack initiation temperature up to 1200 μm; but for increases beyond the 1200 μm limit the crack initiation temperature remains relatively constant. As will be noted from Fig. 6, this trend is the same for all the solder coating thicknesses investigated in our study, although our results discussed earlier in Section 3.1 showed that increasing the solder coating thickness leads to a decrease in the crack initiation temperature. The results presented in Fig. 7 shows that the PV ribbon interconnections experienced a sharp increase in the crack growth rate beyond the 1200 μm

that the crack nucleation location has moved from the IMC layer interface with the copper ribbon (the IMC-Copper) to the IMC layer interface with the silver pad (the IMC-Silver pad). In addition, our results show that the crack locations are now nearer the centre of ribbon interconnect width, but the crack propagation is still in the same shear direction. The location and direction of the initiated crack is in line with the experimental results from previous studies (Jeong, et al., 2012) and (Li, et al., 2009).

Based on the analysis of our results for both the crack initiation temperature and the crack growth rate for the ribbon interconnection geometries investigated, we will advise the use of ribbon interconnect widths of circa 1000 μm, as this will lead to higher ribbon interconnection reliability for the PV module assembly. In addition, this recommendation will also lead to lower materials costs; as increasing
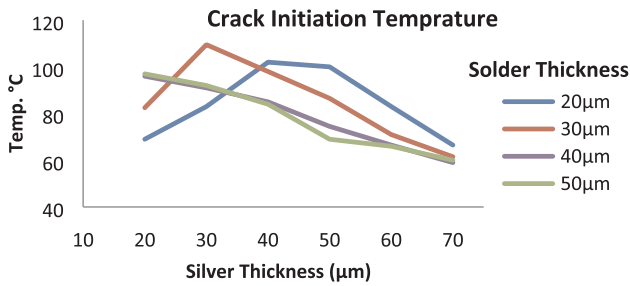
**Fig. 8.** Effect of silver thickness on the crack initiation temperature for different solder thicknesses (Copper thickness, ribbon breadth and IMC thickness are considered as 200 μm, 1 mm and 4 μm, respectively).

the ribbon interconnection width leads to higher metallization and manufacturing costs. In addition to savings on metallization and materials costs, reducing the ribbon interconnection width helps to increase the PV solar module performance as the efficiency of the cell increases with the exposure of more silicon cell surface area to sun light (minimising shading effect).

### 3.3. Effect of silver thickness change

The results presented in Fig. 8 and Fig. 9 show the effect of silver pad thickness on the crack initiation temperature and the crack growth rate for the PV ribbon interconnection geometries investigated in our study. The results show that the crack initiation temperature and the crack growth rate decreases with increasing silver pad thickness. However, Fig. 8 suggests that the crack initiation temperature for 20 μm and 30 μm solder coating thickness peaks at the silver pad thickness in range of 30 μm to 50 μm before it decreases. The results presented in Fig. 9 shows that there is a significant change in the crack growth rate for silver pad thicknesses less than 50 μm; as the crack nucleation is located in the IMC-Silver pad. Based on the results of the ribbon interconnection geometries investigated in our study, the recommended solder coating thickness will be 20 μm, and we recommend silver pad thickness of between 40 μm and 50 μm which will help to achieve a higher ribbon interconnection reliability and reduced material and manufacturing costs.

### 3.4. Effect of change in copper thickness

The results of our study presented in Fig. 10 and Fig. 11 show the effect of copper thickness on the crack initiation temperature and the crack growth rate for the PV ribbon interconnection geometries investigated. The results in Fig. 10 show that increasing the copper thickness leads to a decrease in the crack initiation temperature; and that reduction in the crack initiation temperature is more pronounced for the thicker solder coatings. The results in Fig. 11 also show that the lowest crack growth rate occurs at the 200 μm copper thickness (the lowest point for all solder coating thicknesses). The results also show
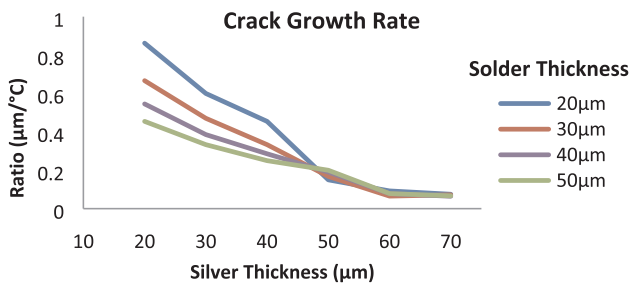


**Fig. 9.** Effect of silver thickness on the crack growth rate for different solder thicknesses (Copper thickness, ribbon breadth and IMC thickness are considered as 200 μm, 1 mm and 4 μm, respectively).
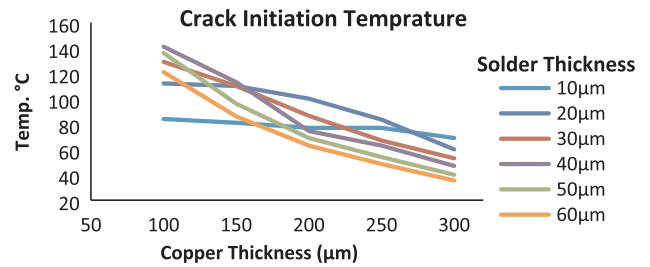


**Fig. 10.** Effect of copper thickness on the crack initiation temperature for different solder thicknesses (Silver thickness, ribbon breadth and IMC thickness are considered as 50 μm, 1 mm and 4 μm, respectively).
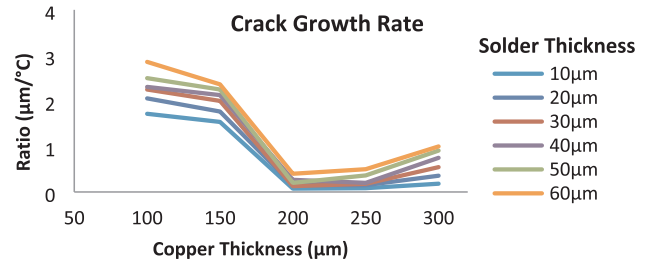


**Fig. 11.** Effect of copper thickness on the crack growth rate for different solder thicknesses (Silver thickness, ribbon breadth and IMC thickness are considered as 50 μm, 1 mm and 4 μm, respectively).

that the PV ribbon interconnection experiences high crack growth rates for the copper thickness below 200 μm, due to crack location in the IMC Layer-Silver pad. Hence, the 200 μm copper thickness is recommended for PV ribbon interconnections as this gives the lowest crack propagation rate and better reliability.

### 3.5. Interaction between copper and silver thickness

Fig. 12 shows the plot of the effect of changing both silver pad and copper thickness on the crack initiation temperature for the PV ribbon interconnection geometries investigated in the study. This shows that reducing the copper thickness leads to an increase in the crack initiation temperature. The results also show that the silver pads with thickness between 40 μm and 50 μm are recommended as this provides the higher crack initiation temperatures and hence better resistance to crack induced failures. Fig. 13 shows the plot of the effect of changing the silver pad and copper thickness on the crack growth rates. The implication of the result in Fig. 13 is that the crack growth rate for smaller silver pad thicknesses is significantly higher when compared with those for thicker silver pads. This is especially true for narrow copper ribbons, as in these cases the crack nucleation location is in the IMC-Silver pad.

### 4. Conclusion

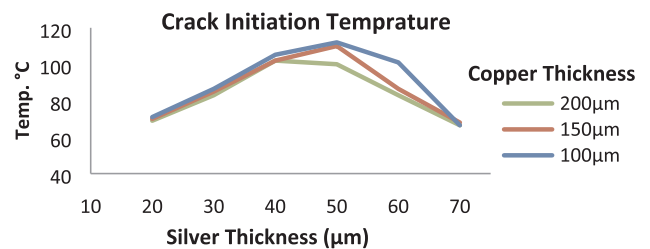In this study, the Extended Finite Element Method (XFEM) in



**Fig. 12.** Effect of silver thickness on the crack initiation temperature for different copper thicknesses (Solder thickness, ribbon breadth and IMC thickness are considered as 20 μm, 1 mm and 4 μm, respectively).
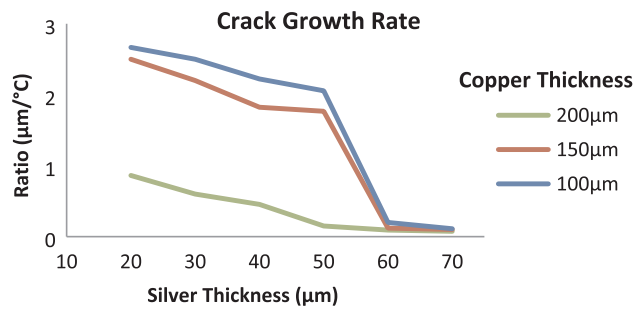
## Crack Growth Rate



**Fig. 13.** Effect of silver thickness on the crack growth rate for different copper thicknesses (Solder thickness, ribbon breadth and IMC thickness are considered as 20 μm, 1 mm and 4 μm, respectively).

ABAQUS 2019 is employed to investigate the effect of geometrical dimensions of the PV module interconnection materials on the micro-crack initiation temperature and the crack growth rate. The results show that the PV module ribbon interconnection configuration has significant influence on the crack initiation temperature and the crack propagation rate; and consequently can adversely affect the PV module interconnection reliability. The results also show that micro-cracks are initiated at the edge of the IMC layer; and that cracks tend to propagate in the shear direction and that crack growth rate is very dependent on the PV module ribbon interconnection geometry.

The main results of the study are summarised below:

- The crack nucleation is located in the IMC layer on the Silver pad side (the IMC-Silver pad) for ribbon interconnect configurations with copper wires widths greater than 1200 μm, with copper wire thickness less than 200 μm and with silver pad thickness less than 50 μm. For other configurations, the crack nucleation is located in the IMC layer on the Copper side (the IMC-Copper). When the crack nucleation location is in the IMC-Silver pad, the crack growth rate is significantly higher, which increases the crack induced failures and adversely affects the reliability of the PV module interconnection.
- Increasing the ribbon interconnection solder coating thickness leads to an increase in the crack growth rate (for solder coatings greater than 50 μm thick) and also a decrease in the crack initiation temperature; and this reduction in crack initiation temperature is more pronounced for thicker IMCs when compared to thinner IMCs. For this reason, a solder coating thickness of between 20 μm and 30 μm is recommended as this will help to keep the crack growth rate low and also keep the crack initiation temperature high; helping to increase the PV ribbon interconnection reliability.
- Increasing the ribbon interconnection width leads to an increase in the crack initiation temperature for widths up to 1200 μm; but the crack initiation temperature remains relatively constant for increases beyond the 1200 μm limit. Based on the analysis of the results for both the crack initiation temperature and the crack growth rate for the ribbon interconnection geometries investigated, we will advise the use of ribbon interconnect widths of circa 1000 μm, as this will lead to higher ribbon interconnection reliability for the PV module assembly. In addition, this recommendation will also lead to reductions in the materials costs; as increasing the ribbon interconnection width leads to higher metallization and higher manufacturing costs. In addition to savings on metallization and materials costs, reducing the ribbon interconnection width helps to increase the PV solar module performance as the efficiency of the cell increases with the exposure of more silicon cell surface area to sun light.
- The crack initiation temperature and the crack growth rate decreases with increasing Silver pad thickness (however, the crack initiation temperature for 20 μm and 30 μm solder coating thickness peaks at the silver pad thickness in range of 30 μm to 50 μm before

decreasing). The recommended solder coating thickness for ribbon interconnections is 20 μm, and we also recommend silver pad thickness of between 40 μm and 50 μm; which will help to achieve a higher ribbon interconnection reliability and reductions in the material and manufacturing costs.
- Increasing the copper thickness leads to a decrease in the crack initiation temperature; and the reduction in the crack initiation temperature is more pronounced for thicker ribbon interconnection solder coatings. The lowest crack growth rate occurs at the 200 μm copper thickness; hence the 200 μm copper thickness is recommended for PV ribbon interconnections as this gives the lowest crack propagation rate and better reliability.

In summary, the results show that the crack initiation temperature and the crack propagation rate are dependent on the dimensions of ribbon interconnection. For the PV module ribbon interconnection configurations and design parameters investigated to establish the impact of interconnection geometry on the crack initiation temperature and crack propagation rate; a ribbon interconnection with 1000 μm copper width, with 200 μm copper thickness, with 50 μm silver pad thickness and with 20 μm solder thickness is recommended for low cost and high reliability PV solar ribbon interconnection.

The methodology developed can be used for investigating the thermal-fatigue life of PV module interconnections subjected to hot/cold service condition and for predicting the long term reliability of the PV solar module based on the knowledge of initial state (existing damage). The results of the study will be beneficial for researchers in predicting the propagation paths for existing micro-cracks during the thermal fatigue cycling under in-service PV module operating conditions; and hence for the predicting of PV Module interconnection reliability.

### Declaration of Competing Interest

The authors declare that they have no known competing financial interests or personal relationships that could have appeared to influence the work reported in this paper.

### Acknowledgment

### Appendix A. Supplementary material

Supplementary data to this article can be found online at https://doi.org/10.1016/j.solener.2020.06.036.

### References

ABAQUS, I., 2017. ABAQUS User's and Theory Manuals; Version 6.17, s.l.: ABAQUS, Inc.: Providence Rhode Island, RI, USA.
Amalu, H.E., Ekere, N.N., 2011. Effects of inter-metallic compound on high temperature reliability of flip chip interconnects for fine pitch applications. s.l., s.n.
Amalu, H.E., Ekere, N.N., 2016. Modelling evaluation of Garofalo-Arrhenius creep relation forlead-free solder joints in surface mount electronic component assemblies. J. Manufact. Syst.
AZoM, 2001. Silver - Applications and Properties of Silver. [Online] Available at: https://www.azom.com/properties.aspx?ArticleID=600.
AZoM, 2005. Aluminium-Specifications, Properties, Classifications and Classes. [Online] Available at: https://www.azom.com/article.aspx?ArticleID=2863.
Bidram, A., Davoudi, A., Balog, R.S., 2012. Control and circuit techniques to mitigate partial shading effects in photovoltaic arrays. IEEE J. Photovoltaics 2 (4), 532–546.
Cambridge University Engineering Department, 2003. Materials Data Book. Cambridge University Engineering Department Data Books, Cambridge.
Deng, X., Sidhu, R.J., Chawla, N., 2005. Influence of reflow and thermal aging on the shear strength and fracture behavior of Sn-3.5Ag Solder/Cu joints. Metall. Mater. Trans. A 36(1), 55–64.
DuPont™, 2014. DuPont™ Tedlar® Polyvinyl Fluoride (PVF) Films. [Online] Available at:

https://www.dupont.com/content/dam/dupont/products-and-services/membranes-and-films/pvf-films/documents/DEC_Tedlar_GeneralProperties.pdf.

Eslami Majd, A., Ekere, N.N., 2019. Numerical analysis on thermal crack initiation due to non-homogeneous solder coating on the round strip interconnection of photo-voltaic modules. Sol. Energy 194, 649–655.

Fei, H., Yazzie, K., Chawla, N., Jiang, H., 2012. Modeling fracture of sn-rich (pb-free) solder joints under mechanical shock conditions. J. Electron. Mater.

Ferrara, C., Philipp, D., 2012. Why Do PV Modules Fail?. Freiburg, Germany, s.n.

Fries, T.-P., 2018. Extended Finite Element Methods (XFEM). Berlin, Heidelberg: Encyclopedia of Continuum Mechanics. Springer.

Hasselbrink, E. et al., 2013. Validation of the PVLife model using 3 million module-years of live site data. Tampa, FL, USA, IEEE 39th Photovoltaic Specialists Conference (PVSC).

Hermann, W., 2010. How temperature cycling degrades photovoltaic-module performance, s.l.: The International Society for optics and photonics (SPIE), doi: 10.1117/2.1201007.003177.

IEA, 2019. Renewables 2019, Paris. [Online] Available at: https://www.iea.org/reports/renewables-2019.

Ishii, T., Atsushi, M., 2017. Annual degradation rates of recent crystalline silicon photovoltaic modules. Prog. Photovolt.: Res. Appl.

Itoh, U. et al., 2014. Solder joint failure modes in the conventional crystalline Si module. s.l., s.n.

Jeong, J.-S., Park, N., Han, C., 2012. Field failure mechanism study of solder interconnection for crystalline silicon photovoltaic module. Microelectron. Reliab.

Jiang, N., Clum, J.A., Chromik, R.R., Cotts, E.J., 1997. Thermal expansion of several Sn-based intermetallic compounds. Scr. Mater. 37 (12), 1851–1854.

Jing, X. et al., 2015. Effect of pre-CMP annealing on TSV pumping in thermal budget and reliability test. Hsinchu, Taiwan, IEEE 22nd International Symposium on the Physical and Failure Analysis of Integrated Circuits.

Lau, H.J., Pan, H.S., Chang, C., 2001. Nonlinear fracture mechanics analysis of wafer level chip scale package solder joints with cracks. Int. Microelectron. Packaging Soc.

Lau, C.-S., Abdullah, M. Z., Mujeebu, M. A., Yusop, N. M., 2014. Finite element analysis on the effect of solder joint geometry for the reliability of ball grid array assembly with flexible and rigid PCBs. J. Eng. Sci. Technol.

Li, J., Karppinen, J., Laurila, T., Ka, J., 2009. Reliability of lead-free solder

interconnections in thermal and power cycling tests. IEEE Trans. Compon. Packag. Technol. 32 (2).

Li, J., Karppinen, J., Laurila, T., Ka, J., 2012. Reliability of lead-free solder interconnections in thermal and power cycling tests. IEEE Trans. Components Packaging Technol. 32 (2).

Moës, N., Dolbow, J., Belytschko, T., 1999. A finite element method for crack growth without remeshing. Int. J. Numer. Meth. Eng. 131–150.

Mohammadi, S., 2008. Extended Finite Element Method: For Fracture Analysis of Structures. Wiley/Blackwell, s.l.

Owen-Bellini, M., Zhu, J., R. Betts, T. Gottschalg, R., 2015. Thermo-Mechanical Stresses of Silicon Photovoltaic Modules. Bangor, United Kingdom, s.n.

Pander, M., Schulze, S.-H., Eber, M., 2014. Mechanical modeling of electrically conductive adhesives for photovoltaic applications. 29th European Photovoltaic Solar Energy Conference and Exhibition.

Pareek, S., Chaturvedi, N., Dahiya, R., 2017. Optimal interconnections to address partial shading losses in solar photovoltaic arrays. Sol. Energy 155, 537–551.

Sander, M., et al., 2011. Investigations on crack development and crack growth in embedded solar cells. Reliab. Photovoltaic Cells, Modules, Components, Syst.

Sasi Kumar, T., et al., 2017. From cells to laminate: probing and modeling residual stress evolution in thin silicon photovoltaic modules using synchrotron X-ray micro-diffraction experiments and finite element simulations. Prog. Photovolt., 25(Research And Applications) 791–809.

Siviour, C.R., Walley, S., Proud, W., Field, J., 2005. Mechanical properties of SnPb and lead-free solders at high rates of strain. J. Phys. D Appl. Phys. 4131–4139.

Taulaukian, Y., Kirby, R., Taylar, R., Desai, P., 1975. Thermal expansion Metallic Elements and Alloys-Thermophysical Properties of Matter Volume 12 Springer Science+Business Media LLC, New York.

Tippabhotla, S.K., et al., 2017. From cells to laminate: probing and modeling residual stress evolution in thin silicon photovoltaic modules using synchrotron X-ray micro-diffraction experiments and finite element simulations: Probing and modeling residual stress evolution. Prog. Photovoltaics Res. Appl. 25, 791–809.

Wang, H., Wang, A., Yang, H., Huang, J., 2016. Study on the Thermal Stress Distribution of Crystalline Silicon Solar Cells In BIPV. s.l., s.n., p. 429 – 435.

Zhong, W., Qin, F., An, T., Wang, T., 2010. Mechanical Properties of Intermetallic Compounds in Solder Joints. s.l., s.n.